Materials Science-Poland, 37(4), 2019, pp. 585-589
http://www.materialsscience.pwr.wroc.pl/
DOI: 10.2478/msp-2019-0069

sciendo

Synthesis and characterization of mesoporous carbon spheres

SHUIPING LI[1,*], HUAJUN ZHU[2], GUILONG XU[2], QING LIN[3], CHENGSHUANG WANG[2], QISHENG WU[2], ZHANHONG WANG[4]

[1]College of Civil Science and Engineering, Yangzhou University, Yangzhou, 225127, P.R. China
[2]School of Materials Science and Engineering, Yancheng Institute of Technology, Yancheng, 224051, P.R. China
[3]School of Materials Engineering, Jinling Institute of Technology, Nanjing, 211169, P.R. China
[4]Analysis and Testing Center, Yancheng Institute of Technology, Yancheng, 224051, P.R. China

A three-step method was used for the synthesis of mesoporous carbon sphere (MCS) material: firstly, silica (SiO_2) nanoparticles were synthesized by the modified Stöber procedure; secondly, tetraethyl orthosilicate (TEOS) and cetyltrimethylammonium chloride (CTAC) were grafted onto SiO_2 core nanoparticles to prepare SiO_2@SiO_2-CTAC hard templates; lastly, MCS material was fabricated by carbonizing and selective leaching SiO_2/resorcinol-formaldehyde (RF) composites. The influence of the mass ratio of R-F/silica on the structure, morphology and crystal form was studied. The results indicate that the MCS materials have a uniform morphology. The increase of the mass ratio of R-F/silica can increase the specific surface area and pore volume. The three-step method provides a cost-effective procedure for the fabrication of MCS materials with uniform morphology.

Keywords: *carbon materials; mesoporous materials; three-step method*

1. Introduction

In recent years, there has been a considerable interest in the preparation of inorganic materials with spherical structure, which was due to their remarkable properties and chemical inertness [1–4]. Especially, mesoporous carbon sphere (MCS) materials with large surface area, appropriate pore volume and excellent mechanical stability, exhibit great potential to be used as a significant class of functional materials for catalysis, electrodes, sensors, etc. [5–8]. There have been several reports focused on the preparation of mesoporous carbon spheres. Li et al. [9] reported a novel approach to the synthesis of carbonaceous materials, which involved creation of mesoporoes in carbon precursor particles by imprinting with colloidal silica particles. Monodisperse resorcinol formaldehyde (RF) resin polymer spheres with finely tunable particle size ranging from 200 nm to 1000 nm were prepared by an extension of the Stöber method [10]. Choma et al. presented an extension of the Stöber method to synthesis of carbon particles, which had micropores, mesopores or both [11].

In the current study, a novel process for synthesis of MCS materials with uniform morphology has been presented. Firstly, silica nanoparticles were synthesized by a modified Stöber procedure; secondly, hard templates of SiO_2@m-SiO_2-CTAC were prepared through the cooperative formation mechanism of CATC and TEOS; finally, MCS materials were fabricated by stirring to generate RF/silica composites in one pot, after which carbonization and selective leaching were performed to obtain the MCS materials. To the best of our knowledge, no study has yet reported the synthesis of MCS materials through this three-step method. This procedure is cost-effective because the carbon source, surfactant and solvent are inexpensive. The obtained MCS materials presented an expected spherical structure and uniform size.

2. Experimental

2.1. Materials

Tetraethyl orthosilicate (TEOS) and resorcinol were purchased from Sinopharm Chemical Reagent Co., Ltd. (Shanghai, China). Hexadecyltrimethylammonium chloride (CTAC)

*E-mail: lishuiping2002@hotmail.com

was obtained from Sigma Aldrich Chemical Reagent Co., Ltd. (St. Louis, America). Aqueous ammonia, formaldehyde and ethanol were supplied by Yixing Tongsheng Chemical Reagent Co., Ltd. (Yixing, China). Hydrofluoric acid was purchased from Yellow River Fine Chemical Company (Xinxiang, China).

2.2. Synthesis of SiO_2 nanoparticles

Silica nanoparticles were synthesized by a modified Stöber procedure using tetraethyl orthosilicate (TEOS) as silica source. 2.5 mL of aqueous ammonia was added to 25 mL of distilled water and stirred for 25 min under magnetic stirring at room temperature (Solution A). 1.5 mL of TEOS was dissolved in 25 mL of ethanol and also stirred for 25 min under magnetic stirring at room temperature (Solution B). Then, solution B was dropped into solution A and the system was kept stirring for 24 h. The white precipitates (SiO_2) were separated by centrifugation, washed with ethanol and water, and dried at 105 °C for 24 h.

2.3. Preparation of SiO_2@SiO_2-CTAC

0.17 g of CTAC was added to the solution containing distilled water (30 mL), aqueous ammonia (0.45 mL) and ethanol (13 mL) under stirring at room temperature. After 15 min, 0.1 g of SiO_2 was added to the solution and the system was kept stirring for 60 min. After that, 1.5 mL of TEOS was dropwise added to the solution under stirring at room temperature. The solution was kept under stirring for 6 h. Then, the precipitates (SiO_2@SiO_2-CTAC) were separated by centrifugation, washed with ethanol and water, and dried in an oven at 105 °C overnight.

2.4. Fabrication of mesoporous carbon sphere materials

0.1 g of SiO_2@SiO_2-CTAC was added to the solution containing distilled water (200 mL), aqueous ammonia (1 mL) and ethanol (20 mL) under stirring at room temperature. After 15 min, 0.8 g of resorcinol was dropped into the solution and stirred for 30 min. Then, 1 mL of formaldehyde was dropped into the solution and stirred for 15 min. The solution was first stirred at 30 °C for 24 h and then at 100 °C for 24. The precipitates (SiO_2/resorcinol-formaldehyde – RF) were separated by centrifugation, washed with ethanol and water, and dried under vacuum at 80 °C overnight.

SiO_2/RF was heated to 600 °C at a heating rate of 2 °C min^{-1} and calcined for 6 h under argon atmosphere. After cooling to room temperature, SiO_2 was removed through selective leaching method by hydrofluoric acid (HF, 4 wt.%). The final product (MCS-10) was washed, centrifugalized and then dried at 80 °C for 24 h under vacuum. Other MCS materials (MCS-15 and MCS-20) were prepared at different molar ratios of R-F/silica, while the other process conditions were kept unchanged. The synthesis route of MCS materials is illustrated in Scheme 1.

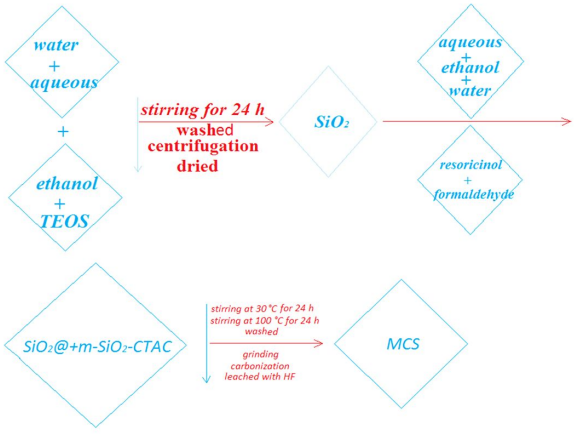

Scheme 1. Synthesis route of MCS materials.

2.5. Characterization

Attenuated total internal reflectance Fourier-transform infrared spectroscopy (ATR-IR) spectra were measured with a Tensor 37 instrument (Germany, Bruker). Each sample was scanned in the range of 400 cm^{-1} to 4000 cm^{-1} (ATR-test, 32 times scanning) with a resolution of 4 cm^{-1}. Field emission scanning electron microscope (FE-SEM) images were recorded by a Hitachi SU 8000 microscope (Hitachi, Japan), and the fracture surfaces of the composites were sputter-coated with gold before observation. FE-SEM photo micrographs were obtained under conventional

secondary electron imaging conditions at an accelerating voltage of 10 kV. High resolution transmission electron microscope (TEM) morphologies were observed by a JEM-2100F (JEOL, Japan) at an accelerating voltage of 200 kV. Samples of powders were suspended in ethanol using an ultrasonic horn, and small volumes of the suspension were deposited onto carbon-coated 400 mesh copper grids and dried under air. Small-angle X-ray scattering (SAXS) patterns were recorded on a X'Pert3 Powder (PANalytical, Netherlands) using CuKα radiation (λ = 0.1540598 nm). N_2 adsorption-desorption isotherms at 77 K were measured with a Tristar II 3020 instrument (Micromeritics, America). The specific surface area was calculated by the Brunauer-Emmett-Teller (BET) method from the linear part of BET plot, according to IUPAC recommendations, using the adsorption isotherm (relative pressure P/P_0 = 0.05 to 0.20). The pore size distribution and pore volumes were calculated by the Barrett-Joyner-Halenda (BJH) method.

3. Results and discussion

FE-SEM images of MCS-10, MCS-15 and MCS-20 and EDS spectrum of MCS-20 material are shown in Fig. 1. As shown in the figure, all the MCS materials have a spherical morphology (Fig. 1a, Fig. 1b and Fig. 1c). MCS-10, MCS-15 and MCS-20 materials exhibit particle sizes of 130 nm to 400 nm, 270 nm to 400 nm and 290 nm to 470 nm, respectively. The SEM images of SiO_2 nanoparticles synthesized using the modified Stöber method are displayed in Fig. 1a, which shows that the size of SiO_2 particles ranges from 300 nm to 700 nm. The sphere sizes of MCS-20 materials are more uniform and larger than those of MCS-10 and MCS-15, which indicates that a high R-F/silica ratio may result in the formation of SiO_2 nanoparticles with uniform size. The EDS spectrum (Fig. 1d) shows that carbon is the main element in MCS-20. The peak of Cu element can be assigned to the copper grid. TEM morphologies of MCS-10, MCS-15 and MCS-20 and microstructure of mesoporous of MCS-20 materials are shown in Fig. 2. It can be seen that all samples exhibit a homogenous size distribution and similar dimensions (Fig. 2a, Fig. 2b and Fig. 2c). Moreover, all MCS materials exhibit an expected excellent spherical morphology. The sphere sizes of MCS materials are close to each other. MCS-10 materials have a particle size of 220 nm to 300 nm. It should be noticed that the particle size of MCS-10 observed by TEM is lower than the size of MCS-10 observed in the SEM images owing to the high resolution of TEM, which can clear distinguish the boundary of MCS particles. However, the TEM image of the microstructure of MCS-20 material presents a disordered mesoporous structure (Fig. 2d), which may result in a low specific surface area. These results indicate that the mass ratio of R-F/silica in the investigated range do not impart any obvious influence on the morphology of MCS materials.

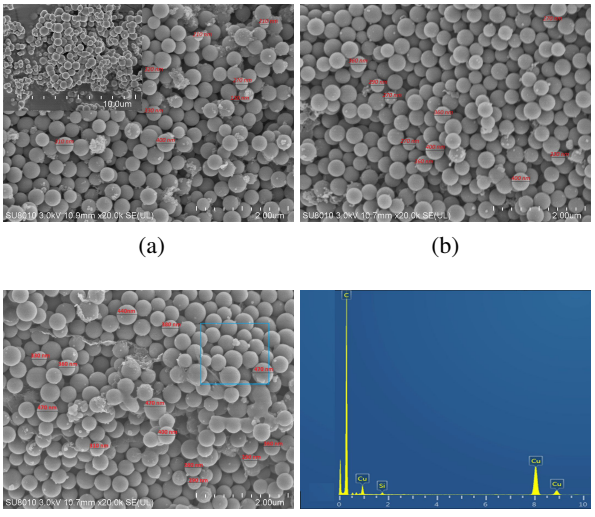

Fig. 1. FE-SEM images of MCS-10 (a), MCS-15 (b), and MCS-20 (c) materials, and EDS spectrum of MCS-20 material (d).

Fig. 3 shows the ATR-IR spectra of MCS-10, MCS-15 and MCS-20 materials. It can be seen that two weak characteristic peaks are present in all these three spectra. The peak at 1588 cm^{-1} can be assigned to the vibration of C=C, which is the characteristic peak of carbon materials. The appearance of the weak peak at 1084 cm^{-1}, which is attributed to the stretching vibration of Si–O–Si, indicates that there are few residues of SiO_2

Table 1. Specific surface area, average pore size and pore volume of MCS materials.

	Specific surface area [m^2/g]	average pore size [nm]	pore volume [cm^3/g]
MCS-10	298	11.9	0.42
MCS-15	435	10.1	0.46
MCS-20	502	9.7	0.52

in the MCS materials. This result is in accordance with the EDS spectrum, which is shown in Fig. 1d.

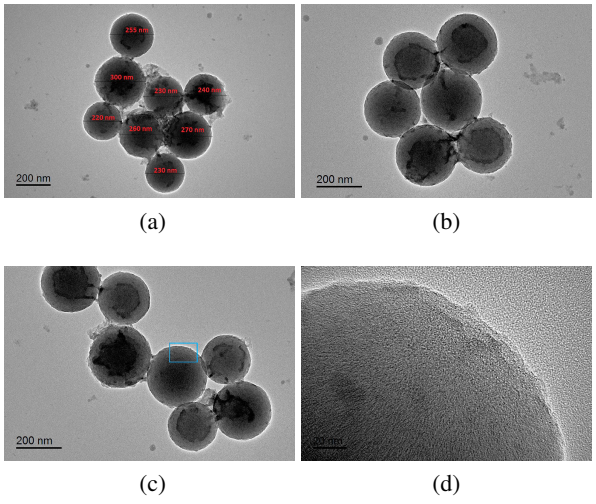

Fig. 2. TEM images of MCS-10 (a), MCS-15 (b), and MCS-20 (c) materials, and a pore structure of MCS-20 material.

N_2 adsorption-desorption isotherms at 77 K of the MCS materials are shown in Fig. 4. The isotherms of MCS materials are all typical of IV isotherms with hysteresis loop, which results from capillary condensation in mesopores. These isotherms show a capillary condensation at a P/P_0 of 0.6 to 0.9, which is characteristic of mesoporous materials [8]. Actually, type IV isotherms are typical isotherms of mesoporous materials according to the IUPAC convention [12]. However, the N_2 adsorption-desorption isotherms do not show an obvious increase in adsorption at a relative pressure P/P_0 of 0.3 to 0.4. This slow increase may exhibit a relative low pore volume [13]. The specific surface areas, average pore sizes and pore volumes of MCS materials are listed in Table 1. Table 1 shows that the specific surface areas of MCS-10, MCS-15 and MCS-20 materials are 298 m^2/g, 435 m^2/g and 502 m^2/g, respectively. The corresponding average pore size and pore volume are 11.9 nm, 10.1 nm and 9.7 nm, and 0.42 cm^3/g, 0.46 cm^3/g and 0.52 cm^3/g, respectively. These results reveal that increasing the mass ratio of R-F/silica can improve the specific surface area and pore volumes but decrease the average pore sizes.

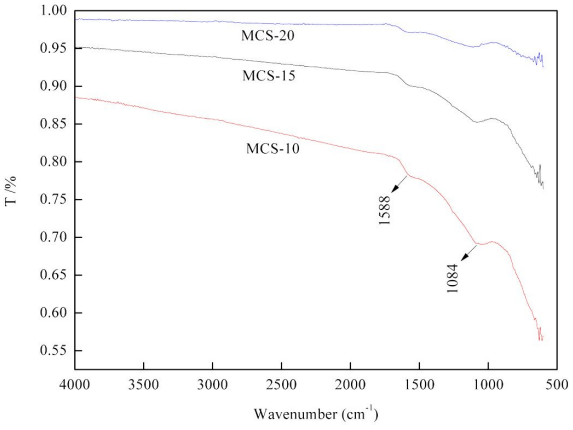

Fig. 3. ATR-IR spectra of MCS materials.

The mesostructural properties of MCS materials were also evaluated by SAXS (Fig. 5). The SAXS patterns of MCS materials present an apparent diffraction peak around $2\theta = 0.85°$, indicating that all the samples have mesoporous pore walls [14]. The patterns do not show an obvious diffraction intensities decrease and diffraction peaks broadening owing to the disordered mesoscopic structure. This result demonstrates that the adjustment of mass ratio of R-F/silica exhibits no obvious influence on the crystal form of MCS materials.

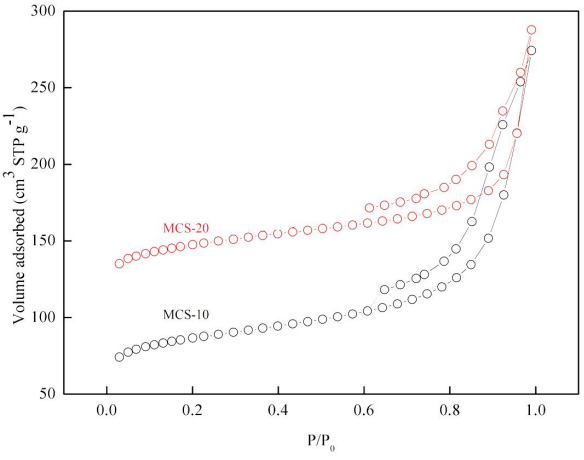

Fig. 4. Nitrogen sorption isotherms of MCS-10 and MCS-20 materials.

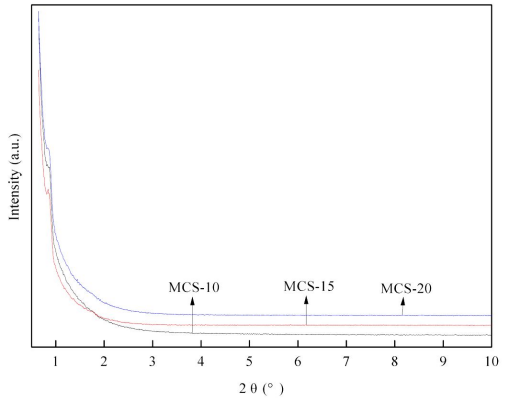

Fig. 5. SAXS patterns of MCS materials.

4. Conclusions

MCS materials were synthesized by three-step method: firstly, a modified Stöber method was used to prepare SiO_2 nanoparticles; secondly, SiO_2@SiO_2-CTAC hard templates were fabricated by grafting of TEOS and CTAC onto the surface of SiO_2 nanoparticles; lastly, hard templates were coated with resorcinol and formaldehyde, followed by carbonization and selective leaching to remove SiO_2 and prepare mesoporous carbon sphere (MCS) materials. The influence of the mass ratio of R-F/silica on the mesostructural properties of MCS materials was investigated using high resolution transmission electron microscope and N_2 adsorption-desorption isotherms at 77 K. The results indicated that increasing the mass ratio of R-F/silica can improve the specific surface area and pore volume but decrease the average pore size. The mass ratio of R-F/silica had no obvious influence on the morphology and crystal form of the MCS materials. However, TEM images showed a disordered mesoporous structure, resulting in a low specific surface area.

Acknowledgements

The authors gratefully acknowledge the financial support of this study by the National Natural Science Foundation of China (51603179), the Six Talent Peaks Project in Jiangsu Province (2017-GDZB-053 and 2016-XCL-070), and the Science and Technology Project from the Ministry of Housing and Urbar-Rural Development of the People's Republic of China 2019-K-061.

References

[1] Zhou J., He J., Zhang C., Wang T., Sun D., Di Z., Wang D., *Mater. Charact.*, 61 (2010) 61, 31.
[2] Wilgosz K., Chen X., Kierzek K., Machnikowski J., Kalenczuk R.J., Mijowska E., *Nanoscale Res. Lett.*, 7 (2012), 269.
[3] Yan Z., Xie J., Zong S., Zhang M., Sun Q., Chen M., *Electrochim. Acta*, 109 (2013), 256.
[4] Zhang L., Kim J., Dy E., Ban S., Tsay K.C., Kawai H., Shi Z., Zhang J., *Electrochim. Acta*, 108 (2013), 480.
[5] Guo L., Zhang L., Shi J., *Mater. Lett.*, 65 (2011), 1.
[6] Tian Y., Zhong S., Zhu X., Huang A., Chen Y., Wang X., *Mater. Lett.*, 161 (2015), 656.
[7] Wang D., Fu A., Li H., Wang Y., Guo P., Liu J., Zhao X.S., *J. Power Sources*, 285 (2015), 469.
[8] Zhong S., Huang W., Tian Y., Wang X., *Mater. Lett.*, 179 (2016), 86.
[9] Li Z., Jaroniec M., *J. Am. Chem. Soc.*, 123 (2011), 9208.
[10] Liu J., Qiao S.Z., Liu H., Chen J., Orpe A., Zhao D., Liu Q.G., *Angew. Chem. Int. Edit.*, 50 (2011), 5947.
[11] Choma J., Jamiola D., Augustynek K., Marszewski M., Gao M., Jaroniec M., *J. Mater. Chem.*, 22 (2012), 12636.
[12] Rojas F., Kprnhauser I., Felipe C., Esparza J.M., Cordero S., Dominguez A., Riccardo J.L., *Phys. Chem. Chem. Phys.*, 4 (2002), 2346.
[13] Li S., Ww Q., Lu G., Zhang C., Liu X., Cui C., Yan Z., *J. Mater. Eng. Perform.*, 22 (2013), 3762.
[14] Liu T., Lai D., Feng X., Zhu H., Chen J., *Ceram. Int.*, 39 (2013), 3947.

Received 2018-08-08
Accepted 2019-04-23